Available online at www.sciencedirect.com
SCIENCE DIRECT
Medical Image Analysis 10 (2006) 642–656
MEDICAL IMAGE ANALYSIS
www.elsevier.com/locate/media

Cardiac function estimation from MRI using a heart model and data assimilation: Advances and difficulties

M. Sermesant [a,b], P. Moireau [c], O. Camara [d], J. Sainte-Marie [c], R. Andriantsimiavona [b], R. Cimrman [e], D.L.G. Hill [d,*], D. Chapelle [c], R. Razavi [b]

[a] INRIA, team ASCLEPIOS, 2004 route des Lucioles, 06902 Sophia Antipolis, France
[b] King's College London, Cardiac MR Research Group, Guy's Hospital, London, UK
[c] INRIA, team MACS, Rocquencourt, France
[d] Department of Computer Science, Centre of Medical Image Computing, University College London, Gower Street, London WC1E 6BT, United Kingdom
[e] University of West Bohemia, Department of Mechanics, Plzeň, Czech Republic

Received 31 January 2006; received in revised form 24 March 2006; accepted 6 April 2006
Available online 12 June 2006

Abstract

In this paper, we present a framework to estimate local ventricular myocardium contractility using clinical MRI, a heart model and data assimilation. First, we build a generic anatomical model of the ventricles including muscle fibre orientations and anatomical subdivisions. Then, this model is deformed to fit a clinical MRI, using a semi-automatic fuzzy segmentation, an affine registration method and a local deformable biomechanical model. An electromechanical model of the heart is then presented and simulated. Finally, a data assimilation procedure is described, and applied to this model. Data assimilation makes it possible to estimate local contractility from given displacements. Presented results on fitting to patient-specific anatomy and assimilation with simulated data are very promising. Current work on model calibration and estimation of patient parameters opens up possibilities to apply this framework in a clinical environment.

Keywords: Cardiac MRI; Myocardium segmentation; Patient-specific model; Cardiac pathologies; Parameter estimation; Data assimilation

1. Introduction

The integration of knowledge from biology, physics and computer science makes it possible to combine in vivo observations, in vitro experiments and in silico simulations. From these points of view, knowledge of the heart function has greatly improved at the nanoscopic, microscopic and mesoscopic scales, along with an impressive development of the observations possibilities.

There are now in vivo modalities to observe the different phenomena involved in cardiac function: mapping of the electrophysiology (Eldar et al., 1997; Schmitt et al., 1999; MacLeod et al., 2001; Faris et al., 2003; Rhode et al., 2005), tracking of the deformation (Axel et al., 2005), measurement of the global and local blood flow velocities (Kilner et al., 2000), or combinations of these (Masood et al., 2000). All these progresses made the design of a global model of the heart conceivable (McCulloch et al., 1998; Geerts et al., 2003; Hunter et al., 2003; Ayache, 2004; Sachse, 2004).

The joint use of imaging and modelling of the heart opens up possibilities in understanding, diagnosis and therapy (see, for instance, the proceedings of the Functional Imaging and Modelling of the Heart conferences (Katila et al., 2001; Magnin et al., 2003; Frangi et al., 2005)). However, due to the limitations of medical imaging, modelling capabilities and computational power, the validation of such heart models with human in vivo data and furthermore their use in clinical applications are still very challenging. The key point in using such models is to be

* Corresponding author.
E-mail address: derek.hill@ucl.ac.uk (D.L.G. Hill).

1361-8415/$ - see front matter © 2006 Elsevier B.V. All rights reserved.
doi:10.1016/j.media.2006.04.002

able to adjust its parameters to patient data in a robust and precise way.

We present in this paper a framework aiming at overcoming these difficulties by directly combining modelling of the heart, cardiac function estimation and parameter adjustment. The aimed application is the estimation of local contractility in the myocardium from displacements measured in medical images.

Estimation of cardiac function from medical images is a very active research area. The main applications in the quantitative assessment of myocardial function are the segmentation of the blood pools (Frangi et al., 2001) and the tracking of the wall motion (Axel et al., 2005). The two main approaches for the segmentation are based on boundaries and regions. The implementation of boundary-based methods can be explicit, with for instance deformable models (Montagnat and Delingette, 2005; Sermesant et al., 2003), or implicit, with for instance level sets (Paragios, 2003; Chenoune et al., 2005). The region-based approach is often a clustering of voxels, with for instance mixture models (Blekas et al., 2005). The tracking of the wall motion can be based on tag lines extraction, deformation models or registration techniques (Chandrashekara et al., 2004; Pan et al., 2005). Ultrasound images also make it possible to estimate cardiac motion (Papademetris et al., 2001) and tissue Doppler gives great insight on motion and flows. Recent real-time 3D probes will help overcoming reconstruction and interpolation artifacts from rotating probes.

Although these tasks give a great insight on the kinematics of the heart, the key factor in many clinical applications is the mechanics of the heart, as this is the most representative of the muscle health and work. To go from the measured kinematics to the actual mechanics, one has to introduce a constitutive law relating both, thus use a model of the myocardium.

The five components presented in this paper are: medical imaging techniques to observe the heart in vivo, building a generic anatomical heart model, adjustment of this generic heart model to patient anatomy, equations used to simulate the cardiac electromechanical behaviour, and data assimilation method to estimate local contractility from displacement. We emphasise in each of these sections the advances made and the difficulties encountered.

To build this framework, a multi-disciplinary collaborative action was needed in order to integrate all the different components, which is an additional difficulty, but such actions can provide new approaches and help for introducing new techniques.

2. Observations: magnetic resonance imaging

Magnetic resonance imaging (MRI) is a successful and promising modality but it remains difficult to use, and the most complex sequences (tags, diffusion tensors) only just start being used outside major research centres. A particular challenge in Cardiac MRI is that the heart is a moving organ, in a moving environment (breathing). This restricts the resolution that can be obtained, and often leads to inconsistent data, making subsequent analysis challenging. Moreover, the acquisition is from several heart cycles, using ECG-gating. This can also create inconsistencies, as many pathologies modify the ECG, due to changes in local conduction. We focus here on the MR imaging techniques for the ventricles.

2.1. Anatomical imaging

Anatomical imaging can be divided in two categories: black-blood and bright-blood. Black-blood imaging is characterised by the suppression of the signal from flowing blood (Simonetti et al., 1996). This gives a good visualisation of the myocardium and enable accurate delineation of myocardial borders with little inter-observer variability (Berr et al., 2005). Unfortunately, due to the pre-pulse and the inversion time, black-blood imaging is not well suited to dynamic (3D+t) imaging. Bright-blood imaging generates high signal intensity for blood and allow both morphological and functional assessment. The recent developments in steady-state free precession (SSFP) based sequences provide high temporal resolution dynamic images with high contrast between the blood and the myocardium in a reduced acquisition time. These sequences have been shown to enable accurate estimation of time-varying intra-ventricular blood volume curve (Kunz et al., 2005). A major drawback however is that delineating the epicardium remains difficult due to the poor or variable contrast between the heart and the other anatomical structures. But we worked with this kind of data, as it is the sequence used clinically for dynamic 3D+t images.

2.2. Functional imaging

2.2.1. Global cardiac function analysis

The quantification of ventricular volumes, myocardial mass and ejection fraction using MRI are both accurate and reproducible in the hand of experienced users (Grothues et al., 2002). However, the time required for acquisition and analysis of MR images hampers the introduction of cardiac MR into routine clinical use. Cardiac MR examinations last frequently more than one hour, and involve numerous breath-holds, which add to patient discomfort.

As mentioned earlier, SSFP bright-blood imaging is a high-quality protocol and is becoming the favoured technique for cardiac function quantification. Fractional k-space filling methods, view-sharing strategies and, most importantly, parallel imaging enable the acquisition time to be considerably reduced without substantial loss of image quality or resolution (Kacere et al., 2005). Alternative approaches for accelerated data acquisition such as kt-BLAST (Tsao et al., 2003) open new paths to extremely fast and rich data acquisition. Despite the development of 3D technology for acquisition, visualisation and

analysis, cardiac MR imaging remains essentially a 2D imaging modality. The major issue with multi-sectional 2D imaging is that the coverage of the ventricles requires multiple breath-holds. Inconsistencies in the different breath-hold positions can lead to errors in image interpretation. Dynamic 3D+t single breath-hold imaging methods appear to be a promising alternative for functional imaging (Peters et al., 2004). Nevertheless, compromises have to be made in terms of image quality, spatial and temporal resolutions.

2.2.2. Regional cardiac function analysis

Ejection fraction is a global parameter that assesses the status of the cardiac function with great sensitivity. However, it is not specific enough for myocardial efficiency and contractility. The study of wall deformations provides more insights on the mechanical contraction of the heart. MR tagging is a well-known method to track local deformations of a "printed" grid as it follows the heart contracting. It enables parameters such as twist, strain and strain rate to be derived (Axel et al., 2005). Although accurate, it is time consuming and suffers from the low spatial resolution of tags. More recently, the development of harmonic phase (HARP, Osman et al., 1999) and displacement encoding stimulated echo (DENSE, Aletras et al., 2005) methods makes it possible to quantify the displacement of each moving pixel inside the myocardium. These techniques though are currently limited to 2D displacements.

The relationship between myocardial motion and contractility cannot be directly estimated from the MR images. Thus, a model-based approach could help to extract this hidden information which is very relevant clinically.

3. Generic anatomical heart model

The aim of this work is to provide a method for model-based analysis of the previously described medical images. The idea is to adjust a biomechanical model of the ventricular myocardium using these images in order to extract hidden parameters useful for diagnosis, like local contractility. To achieve the simulation of cardiac electromechanical activity, we need the myocardium geometry and the muscle fibre orientations as anatomical inputs. The geometry gives the domain on which to carry out computations. Fibre orientations are important for both the active and passive behaviour of the myocardium.

The difficulty for this step is to obtain both types of information for a particular myocardium. On the one hand, geometry can be extracted from anatomical medical images. But fibre orientations cannot be measured in vivo and current diffusion tensor images of fixed hearts are still noisy compared to the smoothness required by the electromechanical computations.

On the other hand, when fibre orientations are measured from dissection, the geometry is often not available, or in so deformed shape that adjustment of the model to the in vivo images becomes very challenging.

Due to these problems, our approach is to synthesise a generic anatomical model of the myocardium, composed of a simple geometry, close enough to in vivo observations, and of synthetic fibre orientations, generated according to the measurements available in the literature (Hsu and Henriquez, 2001; Guccione and McCulloch, 1991).

3.1. Heart geometry

Left ventricle shape is close to a truncated ellipsoid, as shown by the use of this shape for left ventricle volume estimation from 2D images (Mercier et al., 1982). The right ventricle can also be approximated by a truncated ellipsoid. The generic heart model geometry is defined using different parameters for the axis and radii of the left and right ventricles ellipsoids, their thickness and the height of the truncating basal plane (see Fig. 1).

3.2. Heart fibres orientations

It is well known that muscle fibre orientations vary across the myocardial wall. Most diffusion tensor imaging and dissection analysis observed an elevation angle (angle between the fibre and the short axis plane) varying from around $+70°$ on the endocardium to around $-70°$ on the epicardium, depending on the sources (Hsu and Henriquez, 2001; Guccione and McCulloch, 1991), and being horizontal in the short axis plane at mid-wall. Due to the smoothing in the discretisation and averaging per tetrahedron, we analytically defined the fibre image orientation to follow a linear variation between $+90°$ and $-90°$, to obtain the right orientation in the final model.

Fibre have an important impact on the electromechanical behaviour of the myocardium (Ubbink et al., 2006), thus we need to define precisely their orientation and quantify their variability. For the precision, DTMRI gives a more and more precise description of excised hearts, but there are still questions on how precise this must be to correctly compute strain and stress (Ubbink et al., 2006). Recently available DTMRI acquisitions on several excised canine hearts[1] provide a first sample to compute this variability, but a non-trivial registration of these different data sets has first to be performed.

3.3. Cardiac anatomical divisions

Accurate calibration, estimation and analysis of the model is made easier by subdividing it into different anatomical regions. Generating the model makes it possible to analytically divide it into the 17 regions of interest proposed by the American Heart Association (AHA) (Cerqueira et al., 2002).

[1] http://www.ccbm.jhu.edu/research/DTMRIDS.php.

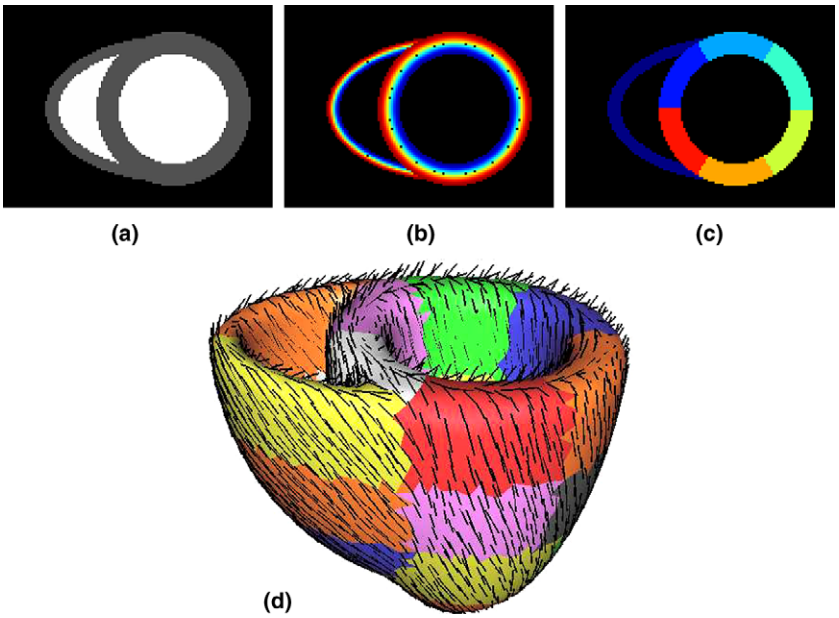

Fig. 1. Generic anatomical bi-ventricular model: equatorial short axis slice of (a) geometry, (b) fibres orientation (elevation angle: red = +90, green = 0, blue = −90), (c) AHA segmental division. (d) Resulting mesh with fibre orientations (black segments) and AHA divisions (colours). (For interpretation of the references to colour in this figure legend, the reader is referred to the web version of this article.)

3.4. Ventricular myocardium mesh

From the anatomical image, a triangulated surface is extracted using the marching cubes algorithm (Lorensen and Cline, 1987). This surface is used to create a tetrahedral mesh with the INRIA GHS3D software.[2] Finally, fibre orientations and subdivisions are assigned to the mesh using rasterisation, see details in (Sermesant et al., 2003). The resulting mesh is presented Fig. 1d.

We typically use meshes with around 4000 nodes and 20,000 tetrahedral elements. This allows to have enough elements to represent well the geometry and the fibre variations, while keeping the mesh small enough for computations. Given the resolution of clinical images, especially the slice thickness, there is no point in using a very fine mesh, which would segment noise and have a stair-case effect after local adjustment.

4. Patient-specific heart anatomy

Automatic segmentation of the myocardium from MRI is still very challenging, and a very active topic (see for instance the approaches proposed in (Mitchell et al., 2002; Paragios, 2003; Lorenzo-Valdés et al., 2004) and references therein for recent references). Additionally, the epicardium is not easily distinguished and the right ventricle is quite thin. Our approach is to deform the generic anatomical model designed in Section 3 into the first 3D image of the sequence. This is done in three steps: segmentation of the image blood pools, intensity-based registration for the affine adjustment and deformable model-based segmentation for local deformations.

4.1. Segmentation of the ventricular blood pools

As stated above, multiple breath-holds SSFP sequences are the most commonly used protocols for cardiac functional imaging. The major benefit of such a sequence is the clear contrast between blood and myocardial tissue. SSFP also presents two other advantages compared to classical gradient echo (GRE) sequences: better signal-to-noise ratio (SNR) and signal intensity persistence over the cardiac cycle. The latter is explained by the fact that the signal is related to the T_2/T_1 ratio rather than the inflowing blood. These particularities are beneficial for "simple" classification-based segmentation algorithms. In clinical context, multi-slices dynamic acquisitions are mostly planned along the plane that cuts the left ventricle transversally (short axis plane). Pixel resolution is often set around 2 by 2 mm and slice thickness usually varies between 7 and 10 mm. If the in-plane resolution provides quite a good separation of the different tissues, the thickness causes an averaging (a "mixing") of the different intensities within the voxels that form the boundaries between tissues – i.e. partial volume effect (PVE).

Based on these image properties, the method that we have developed combines boundary-based and region-based fuzzy classification (Andriantsimiavona et al., 2003) with a probabilistic approach to partition the different classes of tissues mixed in the "partial volumes" (González Ballester et al., 2002). Fig. 2 illustrates some steps and results from this method. An initial region of interest is set around the heart on the first frame (often

[2] http://www-rocq.inria.fr/gamma/ghs3d/ghs.html.

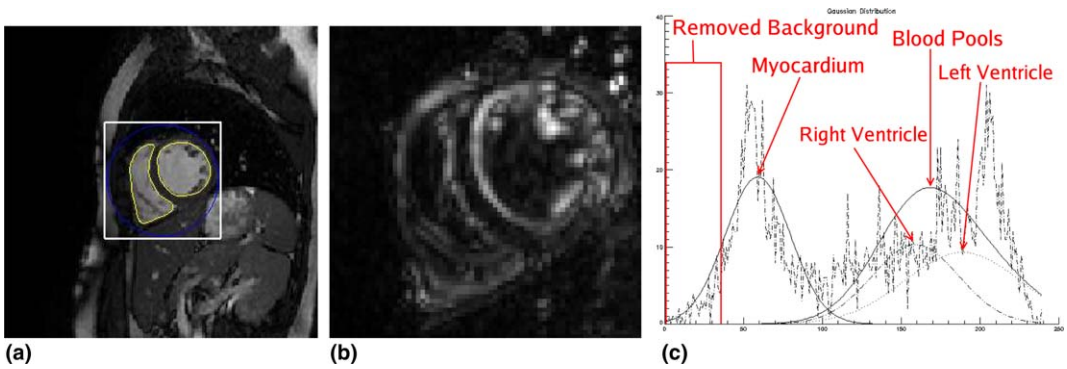

Fig. 2. Segmentation of the ventricular blood pools. (a) Selection of the region of interest (white square) and final segmentation (yellow curve). (b) Variability of pixels intensity during the heart cycle, for one slice. (c) Background removal and first estimation of the Gaussian mixture for myocardium, left and right ventricle blood pools, using the computed variability. (For interpretation of the references to colour in this figure legend, the reader is referred to the web version of this article.)

chosen as end-diastole) of the time series of a slice that is basal enough not to contain much of the papillary muscles or trabeculae. The whole data of the cardiac cycle in that slice is then used to roughly estimate the intensities and locations of the different objects (blood, myocardium and background) to be partitioned. This is based on a statistical separation of pixels between stationary and varying intensities. These initial values are then used as a priori information for a spatially constrained mixture model classification algorithm (Blekas et al., 2005; Liew and Yan, 2003), that separates left and right ventricle from the blood signal and myocardium. The propagation of the segmentation over the different slices uses the previously segmented images as initial guess and a priori knowledge.

4.2. Registration between the model and the image blood pools

The segmentation of the blood pools is then used to estimate the parameters of the ellipsoids that form the generic anatomical heart model. This is to make more robust and more precise the following local adjustment, based on a deformable biomechanical model. Specifically, the bounding boxes enclosing each ventricle are computed to define the length of the ellipsoid axes while their mass centres establish the location of each blood pool ellipsoid. The next step of the affine adjustment involves a principal axes-based registration (Alpert et al., 1990) in which each of the principal orientations of corresponding ventricles (from the model and from the segmentations) are matched. This phase mainly copes with rotations between the segmented blood pools and the model.

Then, an automatic affine (15 parameters) registration algorithm is applied from the segmented image to the blood pools from the model geometry, using the cross correlation as similarity measure. This step is needed to correct possible errors or ambiguities of the principal axes-based registration and to cope with possible remaining scale or shearing differences between the objects to register. Fig. 3 shows the good quality of the affine adjustment obtained with the described procedure prior to the local adjustment.

4.3. Local adjustment using a deformable biomechanical model

Finally, local adjustment is done with a deformable biomechanical model (Sermesant et al., 2003), using the affine transformation computed previously for initialisation. We use a volumetric deformable model with linear elasticity to compute internal forces.

External forces are computed along the normal to the surface nodes. Defining the boundary voxels in the image is made easy by the segmentation, a simple threshold on the gradient value is enough. But it is also necessary to use the gradient direction to distinguish between different boundary voxels, which is very useful for the septum where the deformable model can be confused by the left ventricle and right ventricle endocardial boundaries. When looking for boundaries, one vertex of the mesh can find a close high gradient voxel corresponding to the other side of the myocardium, due to the thin nature of the myocardium. By comparing the normal direction of the mesh surface at this vertex and the gradient direction at this voxel, we can eliminate the high gradient voxels corresponding to the wrong side of the myocardium.

We implemented Houbolt semi-implicit time integration scheme (Bathe, 1996), which gives better results for large deformations: the semi-implicit part regularises the way the mesh deforms. It makes it possible to conserve the good quality of the elements, which is important for the subsequent simulations. As we attach anatomical information to each element (fibre orientation, segment, endocardial/mid-wall/epicardial, basal/apical), it is better to avoid a re-meshing step.

4.4. Results

This whole method allows precise adjustment of the generic anatomical model to the patient image (Fig. 4), but still

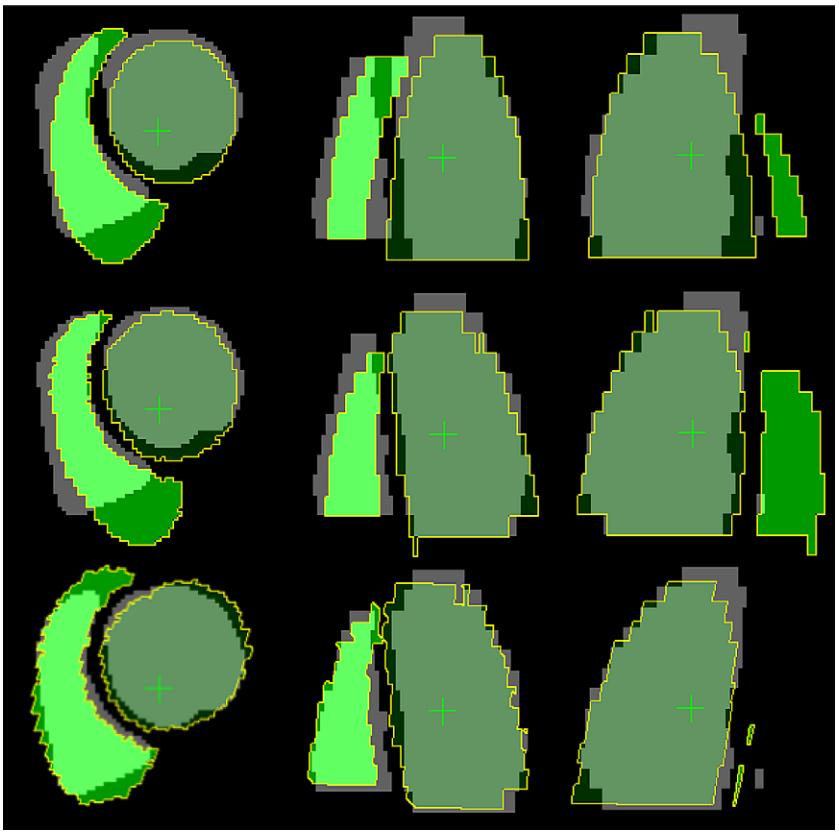

Fig. 3. Registration of the ventricular blood pools between the segmentation (grey) and the model (green) in three orthogonal slices: (top) mass centres alignment, (middle) principal axes alignment, (bottom) affine (15 parameters) registration. (For interpretation of the references to colour in this figure legend, the reader is referred to the web version of this article.)

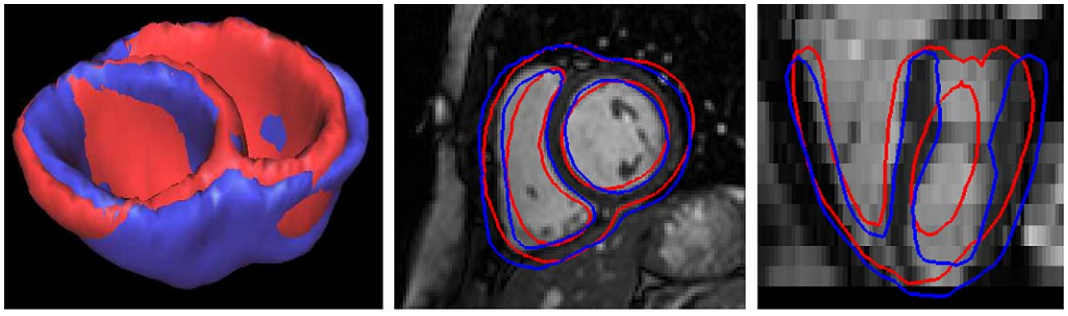

Fig. 4. Local deformation with a biomechanical deformable model. (a) 3D surfaces, (b) short axis and (c) long axis slices of the image and the intersection with the mesh before (red) and after (blue) local deformation. (For interpretation of the references to colour in this figure legend, the reader is referred to the web version of this article.)

preserves surface smoothness and element numerical quality: the aspect ratio mean (resp. standard deviation) on all the tetrahedra of the mesh is 0.674 (0.109) for the original mesh, 0.650 (0.113) after affine transformation, and 0.652 (0.114) after local deformation. We computed a widely used definition of the aspect ratio Q of a tetrahedron, an estimator of the element quality which is defined as the ratio between the radius of the inscribed circle, r_{in}, and the length of the longest edge, $l_{\max}$, in the tetrahedron: $Q = 2\sqrt{6}r_{\text{in}}/l_{\max}$.

To introduce prior information (e.g. fibre orientation) and make it easier to compare the results between normal and pathological cases, it is very advantageous to have correspondence between the reference mesh and patient-specific meshes. Moreover, it is difficult to obtain good quality meshes directly from automatically segmented medical images due to the lack of smoothed boundaries. Therefore we chose to build a generic model and then deform it into the patient-specific data.

The whole process could be rather automated, as segmentation and registration parameters are fairly robust to the variable quality of the input image. The local deformation needs some visual control as no stop criterion has yet been implemented. Nevertheless, from our experience, the parameters in these three steps are quite constant across different images so it should be possible to minimise user input, and the overall time is considerably less than manual segmentation duration. This patient-specific model can then be used for the data assimilation procedure, but there are requirements on the observations used.

A quantitative validation of this segmentation process using manual segmentations is underway.

5. Cardiac muscle biomechanics

Modelling the myocardium behaviour is difficult because of its active, non-linear, anisotropic nature. Several constitutive laws were proposed for the active and passive properties of the myocardium (Katila et al., 2001; Magnin et al., 2003; Frangi et al., 2005).

5.1. Myofibre active constitutive law

An original modelling of the electrically activated myofibres was proposed by Bestel-Clément-Sorine (BCS) (Bestel et al., 2001). Whereas most modelling endeavours rely on heuristic considerations (Arts et al., 2001; Costa et al., 2001; Hunter et al., 2003), the BCS law is based on a multi-scale approach taking into account the behaviour of myosin molecular motors, so that the resulting sarcomere dynamics is in agreement with the sliding filament hypothesis introduced in (Huxley, 1957). Denoting by σ_c the active stress and by ε_c the strain along the sarcomere, this law relates σ_c and ε_c as follows:

$$\begin{cases} \dot{\tau}_c = k_c\dot{\varepsilon}_c - (\alpha|\dot{\varepsilon}_c| + |u|)\tau_c + \sigma_0|u|_+ & \tau_c(0) = 0 \\ \dot{k}_c = -(\alpha|\dot{\varepsilon}_c| + |u|)k_c + k_0|u|_+ & k_c(0) = 0 \\ \sigma_c = \tau_c + \mu\dot{\varepsilon}_c + k_c\xi_0 \end{cases} \quad (1)$$

where u represents the electrical input ($u > 0$: contraction, $u \leqslant 0$: relaxation). Parameters k_0 and σ_0 characterise muscular contractility and respectively correspond to the maximum value for the active stiffness k_c and for the stress τ_c in the sarcomere, while μ is a viscosity parameter.

The propagation of the action potential activating the muscle contraction can be modelled by non-linear reaction-diffusion equations, see (FitzHugh, 1961; Aliev and Panfilov, 1996; Knudsen et al., 1997) and references therein. However, the corresponding numerical computations are costly, and in particular make a combined electromechanical data assimilation procedure well out of reach.

Supposing we are only concerned with diagnosing pathologies independent of electrical activation, we can use pre-computed solutions of activation patterns – for any relevant model – as inputs of our mechanical model. However, if we also aim at estimating quantities associated with electrical pathologies (such as activation isochrones, or depolarization durations), we can use simplified models such as that in (Panfilov and Holden, 1996), for instance. In our approach, we have so far concentrated on the estimation of mechanically related pathologies, and in our simulations we mostly used simplified activation patterns given by a planar wave traveling from apex to base with wave speed v and defined by $u(x,t) = h * [U(t - \frac{x}{v}) - U_{\text{lim}}]$. In this expression U denotes a function representing the transmembrane potential time variations as exemplified in Fig. 5, U_{lim} a threshold value, h a positive constant, and x the coordinate along an axis going from the apex to the centre of the base.

This gives a simplified but easy to compute activation pattern. As compared to mechanical measurements and indicators that we employ in our data assimilation procedure we assume that this simplified electrical modelling is sufficiently accurate. For a complete adjustment of the model, we will need more realistic conduction pathways. We plan to introduce the His bundles and a more realistic Purkinje network. Nevertheless, quantitative data on the localisation of these structures in the human heart is difficult to obtain, in particular due to the fact that they are not visible with imaging.

5.2. 3D model of the myocardium

The above active constitutive law was used within a rheological model of Hill–Maxwell type (Hill, 1938; Chapelle et al., 2001), as depicted in Fig. 6. The element E_c accounts for the contractile electrically activated behaviour governed by Eq. (1). In addition, an elastic material law is considered for the series element E_s, while E_p is taken viscoelastic. Based on experimental results, the corresponding stress–strain laws are assumed to be of exponential type for E_p (Veronda and Westmann, 1970). The stress–strain law for E_s – which plays an important role during isovolumetric phases – is generally assumed to be linear (Mirsky and Parmley, 1973), and we follow this assumption in our modelling. The role of E_p, described in more detail below, is in particular to prevent the heart from overstepping certain limits during filling and ejection.

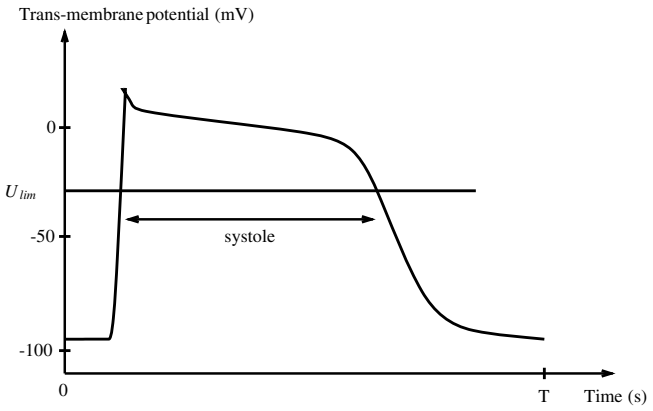

Fig. 5. Transmembrane potential along a cardiac cycle.

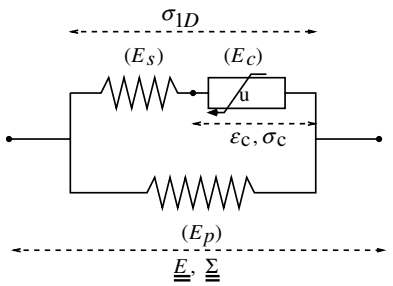

Fig. 6. Hill–Maxwell rheological model.

This rheological model is compatible with large displacements and strains and led to a continuum mechanics description of the cardiac tissue (Chapelle et al., 2004). A study and simulations of a simplified 1D model derived from this continuum mechanics model are detailed in (Chapelle et al., 2001). The equations of the 3D model are summarised in the fundamental equation of continuum mechanics known as the *principle of virtual work*, which is expressed in a total Lagrangian formulation as

$$\int_\Omega \rho \ddot{\underline{y}} \cdot \underline{v}\, d\Omega + \int_\Omega \underline{\underline{\Sigma}} : \delta \underline{\underline{E}}\, d\Omega + \int_{\Gamma_{El} \cup \Gamma_{Er}} P_v \underline{y} \cdot \underline{\underline{F}}^{-1} \cdot \underline{v} \det \underline{\underline{F}}\, d\Gamma = 0 \quad \forall \underline{v} \in V_0 \tag{2}$$

In this equation, Ω denotes the reference domain corresponding to cardiac tissue, while the part of the boundary corresponding to ventricular endocardium is denoted by $\Gamma_{El} \cup \Gamma_{Er}$ (referring to the left and right ventricles), $\underline{v}$ being defined as the outward unit normal vector for this boundary. The main unknown in Eq. (2) is the field $\underline{y}$ that represents the displacement from the reference to the current (deformed) configuration along time. Note that the first integral contains the inertia term $\rho\ddot{\underline{y}}$, ρ denoting the mass per unit volume (in the reference configuration). The deformation gradient $\underline{\underline{F}}$ is defined as $\underline{\underline{F}} = \underline{\underline{I}} + \nabla \underline{y}$, where $\underline{\underline{I}}$ denotes the identity tensor and ∇ the gradient operator. $\det \underline{\underline{F}}$ is the Jacobian of the transformation.

We point out that Eq. (2) is valid for an arbitrary virtual displacement field $\underline{v}$ taken in the space of test functions V_0, and $\delta \underline{\underline{E}}$ denotes the corresponding linearised variation of Green–Lagrange strain. Namely, $\delta \underline{\underline{E}}$ corresponds to the first order term in $\underline{v}$ in the expansion of $\underline{\underline{E}}(\underline{y} + \underline{v})$, where we recall that $\underline{\underline{E}}(\underline{y})$ is defined by $\underline{\underline{E}}(\underline{y}) = 1/2(\underline{\underline{F}}^T \cdot \underline{\underline{F}} - \underline{\underline{I}})$.

The complex electromechanical behaviour discussed above enters in the expression of the second Piola–Kirchhoff stress tensor

$$\underline{\underline{\Sigma}} = \underline{\underline{\Sigma}}_p + \sigma_{1D} \underline{n} \otimes \underline{n}$$

where the first term represents the passive (viscoelastic) behaviour due to element E_p (recall Fig. 6), while σ_{1D} corresponds to the contractile behaviour, including σ_c defined in Eq. (1), and occurring along the fibre direction as characterised by the unit vector $\underline{n}$ (the symbol $\otimes$ denoting tensorial products).

In E_p we consider a viscoelastic behaviour, namely,

$$\underline{\underline{\Sigma}}_p = \frac{\partial W^e}{\partial \underline{\underline{E}}} + \frac{\partial W^v}{\partial \dot{\underline{\underline{E}}}},$$

where W^e and W^v, respectively, represent a hyper-elastic potential and a viscous pseudo-potential. Considering the nearly incompressible character of the material we used a Mooney–Rivlin material (Le Tallec, 1994) in W^e, as is frequently encountered in the literature of biological tissues. For alternative choices, see e.g. (Fung, 1993; Humphrey, 2002; Veronda and Westmann, 1970; Mulquiney et al., 2001; Lin and Yin, 1998) and references therein. The viscous part was modeled by the simple law:

$$W^v = \frac{\eta}{2} \mathrm{Tr}(\dot{\underline{\underline{E}}})^2$$

We refer to (Sainte-Marie et al., in press) for a more detailed description and discussion of the mechanical modelling.

Finally, the quantity P_v featured in the last term of Eq. (2) denotes intra-ventricular pressure, which will be discussed in the forthcoming section.

5.3. Modelling the blood

The blood inside each ventricle is modelled as a pressure/volume system. The phases of the cardiac cycle (isovolumetric contraction, ejection, isovolumetric relaxation, filling) are distinguished through coupling conditions between the internal fluid and other parts of the cardiovascular system, namely the atrial cavities and the external circulation. With P_v, P_{ar} and P_{at} denoting the blood pressures in the ventricle, the artery, and the atrium, respectively, the ejection occurs when $P_v \geqslant P_{ar}$ whereas the mitral valve opens when $P_v \leqslant P_{at}$, see Fig. 7a. Denoting by Q the

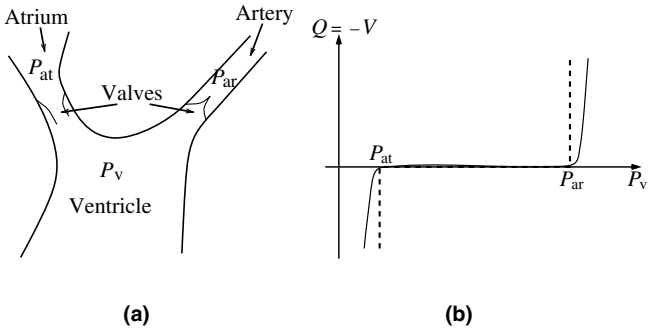

Fig. 7. (a) Aortic valve model mechanism. (b) Formulation as a double contact problem, dashed: relation (3), solid: regularised.

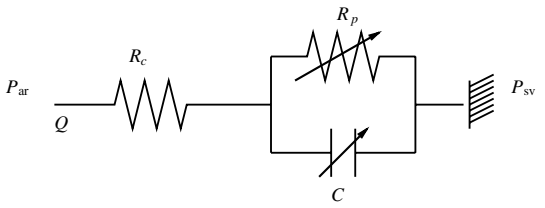

Fig. 8. The 3-element Windkessel model.

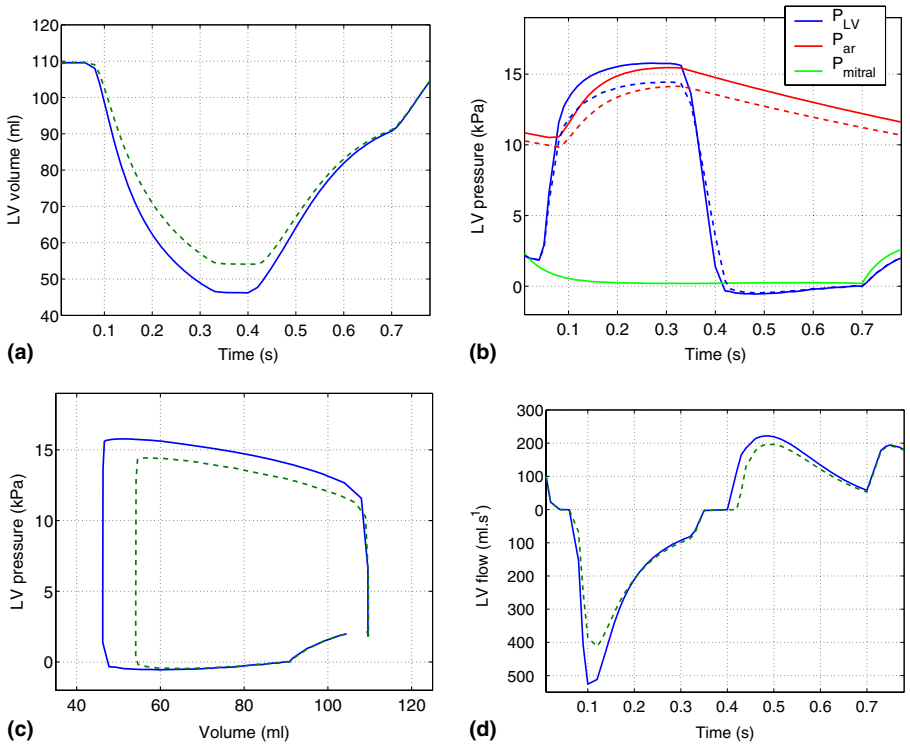

Fig. 9. Computed medical indicators for the left ventricle in reference (solid line) and pathological cases (dashed): volume variations, blood pressures, pressure-volume diagram, inflow and outflow (positive and negative values, respectively).

outgoing flow, the coupling conditions can be formulated as a (double) contact problem:

$$\begin{cases} Q \geqslant 0 & \text{when } P_{\mathrm{v}} = P_{\mathrm{ar}} \quad \text{ejection} \\ Q = 0 & \text{when } P_{\mathrm{at}} < P_{\mathrm{v}} < P_{\mathrm{ar}} \quad \text{isovolumetric phases} \\ Q \leqslant 0 & \text{when } P_{\mathrm{v}} = P_{\mathrm{at}} \quad \text{filling} \end{cases} \tag{3}$$

To avoid numerical difficulties, we used a regularised form of this function as depicted by the solid line in Fig. 7b.

While the blood flow coming from the atria was modelled by a prescribed pressure P_{at}, we used a so-called Windkessel model to represent the arterial flows. Windkessel models can be derived from electrical circuit analogies where current and voltage represent arterial flow and pressure, respectively, see (MacDonald, 1974; Stergiopulos et al., 1999). In our simulations, we used the three-element model depicted in Fig. 8. The corresponding pressure–flow relation reads

$$C\dot{P}_{\mathrm{ar}} + \frac{P_{\mathrm{ar}} - P_{\mathrm{sv}}}{R_{\mathrm{p}}} = \left(1 + \frac{R_{\mathrm{c}}}{R_{\mathrm{p}}}\right) Q + R_{\mathrm{c}} C \dot{Q} \tag{4}$$

and is only valid during ejection, namely when $Q > 0$. During isovolumetric phases and ventricular filling, arterial pressure is instead described by

$$C\dot{P}_{\mathrm{ar}} + \frac{P_{\mathrm{ar}} - P_{\mathrm{sv}}}{R_{\mathrm{p}}} = 0 \tag{5}$$

In the above equations the parameter P_{sv} denotes a fixed "remote" low pressure (typically the venous system pressure for the left compartment).

This three-element Windkessel model has been found to be in good agreement – after proper adjustment of the resistance and capacitance parameters – with clinical measurements. In Fig. 8 the arrows for C and R_{p} indicate that these quantities can be varied to account for nervous system regulation.

We point out that we use two different such Windkessel models (with different resistance and capacitance parameters, of course) to represent the systemic and pulmonary circulations, without connection between the two. This is justified within the time scale that we consider, namely, we are concerned with phenomena that take place within one single cycle. Conservation of blood volumes between the two compartments occurs only at larger time scales, indeed.

5.4. Results

The integration of the described model using the finite element method makes it possible to simulate normal and pathological cardiac function. The finite element implementation was performed within the OpenFEM toolbox.[3] The simulation time for a complete cardiac cycle is approximately one hour on a standard PC. The resulting global cardiac function parameters are presented in Fig. 9.

The calibration of the mechanical parameters featured in the model was performed using physiological and mechanical considerations regarding the meaning and

[3] http://www.openfem.net.

Table 1
Values of the parameters used for the reference situation

α	1
μ	200 (Pa s^{-1})
k_0	3.5×10^5 (Pa)
σ_0	7×10^5 (Pa)
ξ_0	*0*
h	*0.25*
U_{lim}	−30 (mV)
v	3 (m s^{-1})
ρ	1×10^3 (kg m^{-3})
μ	600 (Pa s^{-1})
$P_{ar}(0)$	10 (kPa)
E_s	5×10^6 (Pa)
C	87×10^{-4} (l Pa^{-1})
R_p	1.15×10^{-6} (Pa l^{-1} s)
R_c	0.05×10^{-6} (l Pa^{-1} s^{-1})
P_{sv}	1 (kPa)
$P_{ar}(0)$	10 (kPa)
T	0.8 (s)

effects of each parameter. For example the viscosity of the passive part of the constitutive law is related to the speed of relaxation of the heart during filling whereas the hyperelastic coefficients are directly linked to the relaxation level. The resulting global cardiac function indicators are presented in Fig. 9. The values of the parameters used for the reference simulation are given in Table 1.

We obtain realistic simulation of global kinematics (volume) and mechanics (pressure) of the cardiac function. The data assimilation procedure described below will make it possible to further validate the model and estimate more precisely the parameters with the available patient data.

A pathological case was also simulated: a reduced contractility was chosen for two different anatomical segments (see Fig. 10). This could correspond to an ischemic area in the myocardium, where the muscle does not contract well anymore. The simulated pathological cardiac function is altered in the expected way: significantly reduced ejection fraction and blood pressure.

6. Estimation of local contractility from displacement

The aim of data assimilation is to incorporate measurements into a dynamic system model in order to produce accurate estimates of the current (and possibly future) state variables, parameters, initial conditions and input of the model.

6.1. Data assimilation algorithm

The symbol H denoting the observation operator, $Y(t)$ the available measurements and $X(t)$ the model response, the general objective of data assimilation is the minimisation of a cost function J (objective function) performed over the set of parameters to be estimated

$$J = \int_I \|Y(t) - HX(t)\|_\Omega^2 \, dt + \text{penalty} \tag{6}$$

where $\|.\|_\Omega$ represents a suitable norm associated with the problem formulation.

If I denotes the complete simulation time interval $[t_0, T]$, the assimilation technique is said to be variational and corresponds to an optimal control problem (Le Dimet and Talagrand, 1986; Courtier and Talagrand, 1987; Lions, 1968). If at each time step t_k, $I = [t_0, t_k]$, then the filtering technique is said to be sequential (Kalman, 1960; Kalman and Bucy, 1961). These approaches were used in various applications (Chui and Chen, 1999; Kellerhals, 2001; Kano et al., 2001).

For our problem, the sequential approach is conceptually possible, but the associated covariance matrix required is full with a size (namely, the number of degrees of freedom in the simulation plus the dimension of the parameter space) which makes it intractable for the 3D problem without resorting to specific reduction methods.

Variational data assimilation techniques are based on an iterative approximation of the optimality condition $\nabla_\theta J(\theta^*) = 0$, where θ denotes the parameter set to estimate, leading to an adjoint problem. If the problem to solve is (A), the adjoint state P is governed by (B):

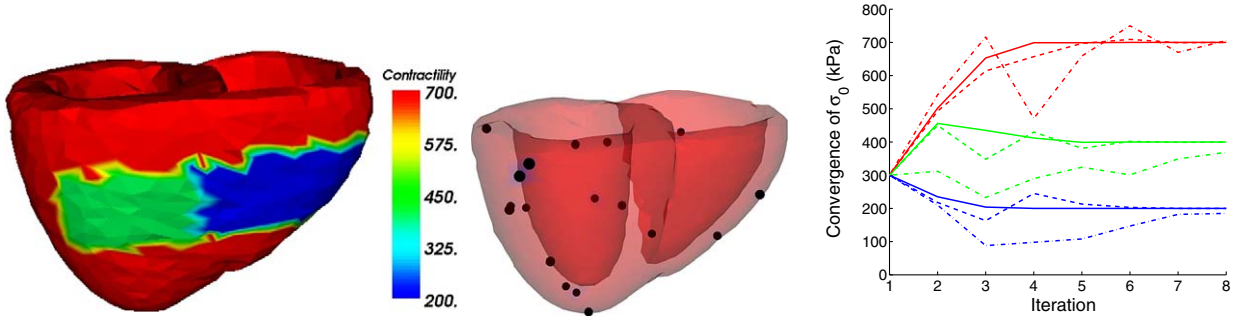

(a) Reference σ_0 **(b)** Measure Points **(c)** Estimated σ_0

Fig. 10. Estimation of reduced contractility values in two AHA segments. (a) Reference values presented on the mesh, (b) 18 random points used as measures in the data assimilation, (c) convergence of σ_{0_j} along iterations of the data assimilation, (—) without noise, (--) with 5% noise, (-·) with 15% noise. The reference values of the contractility in the three areas are $\sigma_{0,1} = 700$, $\sigma_{0,2} = 400$ and $\sigma_{0,3} = 200$ (in kPa), $k_0 = \sigma_0/2$ in all areas.

$$(\mathrm{A})\begin{cases}\dot{X}=F(X,\theta,t)\\ X(t_0)=X_0\\ \theta \text{ unknown parameters}\end{cases}\qquad(\mathrm{B})\begin{cases}\dot{P}+\left[\frac{\partial F}{\partial X}\right]^t P=H^t(HX-Y)\\ P(T)=0\end{cases}$$

The general algorithm used is the following:

- Start from a first guess θ° of the parameter set
- Start iteration n
  - Integrate the direct model from 0 to T
  - Integrate the adjoint model from T to 0
  - Calculate the gradient $\nabla J(\theta^n)=-2\int_0^T P^t\left[\frac{\partial F}{\partial \theta^n}\right]\mathrm{d}t$
  - Compute $\theta^{n+1}=\theta^n+\rho_n\nabla J(\theta^n)$
- $n\rightarrow n+1$ until a stopping criterion on J is reached

The computation of the gradient using the adjoint problem is very effective in the case of multiple parameter estimation, since it provides the complete gradient with one single (backward) time integration. However, it requires the storage of the direct problem solution at all time steps.

The data assimilation process outlined below, which was already used in (Rohan and Whiteman, 2000), and described for biomechanical models in (Rohan and Cimrman, 2002), uses an alternative procedure to compute the gradient using direct differentiation instead of the adjoint problem.

The state problem is given by the finite element discretisation of Eq. (2), and solved for $t=0,\ldots,T$. Here we denote it by $\Phi^{(t)}(\theta,y_t,y_{t-1})=0$, to stress its dependence on the vector of parameters to identify ($\theta\in\mathbb{R}^{\mathbb{m}}$), and on the current and previous state vectors (y_t, y_{t-1}). In our case y is the vector of nodal displacements. Writing the problem in this time-discretised manner makes easier the direct differentiation described below. Let I now be the index subset of the time steps where measurements $(\bar{\varphi}_i)_{i\in I}$ are available, and $\varphi_i(\theta,y_i)$ be the corresponding simulated values of the observed quantity (displacements).

A Newton-type method was used to perform the identification, which is in fact a solution to the following nonlinear least-squares problem (NLS), seeking the vector θ_{aim} of the parameters:

$$\theta_{\mathrm{aim}}=\mathrm{argmin}\left\{J(\theta)|\theta=\{\theta_i\}_{i=1}^n\in\mathbb{R}^n\right\} \tag{7}$$

where the objective function J is discretised as:

$$J(\theta)=\frac{1}{2}\sum_{i\in I}(\varphi_i(\theta,y_i)-\bar{\varphi}_i)^2 \tag{8}$$

with the constraints that the model equations are respected:

$$\Phi^{(0)}(\theta,y_0)=0,\qquad \Phi^{(t)}(\theta,y_t,y_{t-1})=0,\quad t=1,\ldots,T \tag{9}$$

and that parameters keep values compatible with physiological knowledge:

$$\theta_i^{\min}<\theta_i<\theta_i^{\max}\ \text{for some } i$$

Such a minimisation method works best when the gradient of the objective function is available. To compute this gradient, it is necessary to carry out a sensitivity analysis, where we obtain the derivatives of the model with respect to its parameters.

The total (sub)gradient of J is:

$$\nabla_\theta J=\sum_{i\in I}(\varphi_i(\theta)-\bar{\varphi}_i)\nabla_\theta\varphi_i\quad\text{and}$$

$$\nabla_\theta\varphi_i=\frac{\partial\varphi_i}{\partial\theta}+\frac{\partial\varphi_i}{\partial y_i}\,\frac{\partial y_i}{\partial\theta} \tag{10}$$

In our case, the observation operator is constant and corresponds to extracting the nodes where we have measured displacement, so $\frac{\partial\varphi_i}{\partial\theta}=0$ and $\nabla_\theta\varphi_i$ is just a selection of rows of $\frac{\partial y_i}{\partial\theta}$ corresponding to the measured displacements.

We still need to know how to compute $\frac{\partial y_i}{\partial\theta}$. But as it is a minimisation with the constraint that the model equations are respected, we can obtain the gradients $\frac{\partial y_i}{\partial\theta}$ of the (unknown) solution by differentiating Eq. (9):

$$\frac{\partial\Phi^{(t)}}{\partial\theta}+\frac{\partial\Phi^{(t)}}{\partial y_t}\,\frac{\partial y_t}{\partial\theta}+\frac{\partial\Phi^{(t)}}{\partial y_{t-1}}\,\frac{\partial y_{t-1}}{\partial\theta}=0,\quad t=1,\ldots,T \tag{11}$$

$$\frac{\partial\Phi^{(0)}}{\partial\theta}+\frac{\partial\Phi^{(0)}}{\partial y_0}\,\frac{\partial y_0}{\partial\theta}=0 \tag{12}$$

We thus obtain a recurrence relation that allows us to compute $\frac{\partial y_i}{\partial\theta}$. With the notations $x^{(t)}\equiv\frac{\partial y_t}{\partial\theta}$, $V^{(t)}\equiv\frac{\partial\Phi^{(t)}}{\partial\theta}$, $P^{(t)}\equiv\frac{\partial\Phi^{(t)}}{\partial y_t}$, $W^{(t)}\equiv\frac{\partial\Phi^{(t)}}{\partial y_{t-1}}$, the sensitivity analysis is the step two of the following parameter estimation algorithm:

(1) call the nonlinear least squares (NLS) with $\theta=\theta^\circ$
(2) start iteration n:
  (a) perform the sensitivity analysis for θ^n:
    - for time step 0:
      - solve state problem $\Phi^{(0)}(\theta^n,y_0)=0$
      - from $P^{(0)}x^{(0)}=-V^{(0)}$ obtain $x^{(0)}$
    - for time steps $t=1,\ldots,T$:
      - solve state problem $\Phi^{(t)}(\theta^n,y_t,y_{t-1})=0$
      - from $P^{(t)}x^{(t)}=-(V^{(t)}+W^{(t)}x^{(t-1)})$ obtain $x^{(t)}$
      - if exists observation $\bar{\varphi}_t$: evaluate observation function $\varphi_t(\theta^n,y_t)$ compute gradient $\nabla_\theta\varphi_t=\frac{\partial\varphi_t}{\partial\theta}+\frac{\partial\varphi_t}{\partial y_t}\,x^{(t)}$
    - return $\varphi_i(\theta^n,y_i)-\bar{\varphi}_i$ and $\nabla_\theta\varphi_i$ to NLS
  (b) compute new θ^{n+1}
  (c) $n\rightarrow n+1$ until a stopping criterion is reached
(3) return the identified θ

The data assimilation is achieved by performing this iterative algorithm. Note that the proposed algorithm is computationally very effective for a limited number of unknown parameters. Indeed, each NLS step only requires one time simulation for the state and for each of the sensitivity quantities $\frac{\partial y_t}{\partial\theta}$ (one for each independent scalar parameter to be estimated). In addition, at each time step all the sensitivities satisfy a *linear system* with the same governing matrix, see Eq. (11), hence only one matrix inversion is required.

In the following results, the parameter set to adjust is local contractility in different anatomical segments ($\theta = \sigma_0(M)$).

6.2. Results

Preliminary results in data assimilation have been presented in (Sainte-Marie et al., 2003). Results presented here have been obtained using numerically simulated observations assimilated with the complete 3D problem on a realistic heart model (Fig. 10). Due to the complexity of the model and to observability considerations, estimating all the quantities appearing in the complete electromechanical problem is out of reach. Hence we focus on parameters that are crucial for medical purposes in order to detect contraction troubles, in particular the contractility parameter σ_0. Moreover, to be able to achieve such computations, it is important to cluster the parameters, as trying to estimate a parameter for each node would not be tractable. This is why anatomical segments are important, as they provide a first division of the myocardium, which can be refined if necessary. Then only a parameter per segment, or group of segments, is estimated.

These results were obtained as follows:

(1) The direct 3D problem is simulated with a given parameter $\sigma_0(M)$, varying across different anatomical segments (700, 400, 200 kPa).
(2) Observations $(\bar{\varphi}_i)_{i\in I}$ are obtained using the displacements for 18 random nodes of the mesh plus one node in each modified contractility region, with [0, 5, 15]% noise added to these displacements.
(3) Starting from a given parameter $\theta^0 = \hat{\sigma}_0$ different from the one used for the direct simulation (300 kPa), the data assimilation is carried out. The simulated measurements are used at half the frequency of the simulations: simulations are carried out with a 5×10^{-3} s time step, but the measurements are only used every 10^{-2} s.

For this simulation we chose $\sigma_0(M)$ constant across the wall, with three regions of different σ_0, visible on Fig. 10a. The result of the estimation of σ_0 is shown in Fig. 10b. The data assimilation process, initialised with a homogeneous distribution, recovered the spatial variations of σ_0 rather accurately. We used the variational technique described in the previous section. The stopping criterion is a 10^{-4} tolerance on θ ($\|\theta^n - \theta^{n+1}\| < 10^{-4}$), and convergence is achieved in 8 iterations.

We obtain very promising results on simulated data. Even with added noise of 15%, it still converges to the right values. But before applying this technique to real data, several difficulties have to be tackled, which will be discussed in the following section.

6.3. Data assimilation difficulties

Measurements used to apply the data assimilation in Section 6 are displacements in some points within the myocardium muscle. The idea is to use the same data assimilation procedure, with displacements from tagged MRI.

In data assimilation, difficulties arise from various areas, from the available measurements to the complexity of the operator (type of variables, dimension, rank) and the natures of the spaces and norms used. Current work on these difficulties should help design the best possible operators to achieve this parameter estimation.

The first step before running data assimilation on MR-based displacements is to calibrate the model for the given data set. Indeed, there are several parameters in the model that are patient-specific, and we must design ways to adjust them before hand. For instance pre-load and after-load (which correspond to blood pressure in atria for filling and arteries for ejection) play an important role in cardiac function, and they appear in the model. Recent advances both in MR flow measurements and fluid-structure models of the vessels open up possibilities to evaluate these boundary conditions.

A mathematical difficulty of data assimilation is the invertibility of the observation operator H because we want to obtain the state X and the parameters from the observations using a generalised inverse of H. The analysis of this invertibility property (observability) is very difficult in general with respect to both surjectivity (whether there exists a set of parameters and variables which leads to the given observation) and injectivity (whether this set is unique).

Another difficulty in the choice of the observation operator lies in the fact that the efficiency of the data assimilation technique is highly dependent on the noise. To avoid the accumulation of the errors of the different image processing steps, an idea could be to formulate an operator as close to the measurements as possible. We could consider the tagged images as the observation by simulating tagged images from the model displacements. We present in Fig. 11 the simulation of a short axis tagged image compared with the acquired tagged image, in end diastole. To achieve this, a binary image of the mesh is created using rasterisation (Sermesant et al., 2003), tag lines are added to this image, and simulated displacement are interpolated in each tetrahedron to compute the deformed image. Further comparison of these images and design of the

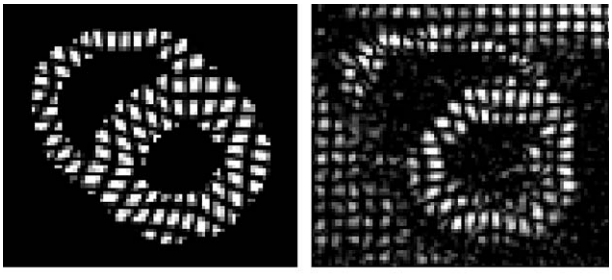

Fig. 11. Simulation of tagged MRI using the deformation from the electromechanical model. (a) Simulated image (short axis slice, end systolic), (b) acquired image.

corresponding observation operator is in progress. For instance, to improve this comparison, recent full 3D tagged MRI could allow to directly work in 3D (Ryf et al., 2002), as the model is 3D.

7. Conclusion and perspectives

This paper presented the adjustment of a generic myocardium model to a patient-specific anatomy using MRI, and a framework to automatically estimate mechanical parameters, like local contractility, from displacements. We detailed: the medical images clinically used and the information we can extract from it; the construction of a generic anatomical model of the ventricular myocardium integrating muscle fibre orientations and anatomical segments; the fitting of this model to patient anatomy; the biomechanical modelling of the myocardium; and a data assimilation method to automatically adjust the parameters of the model from known displacements. We demonstrated the capability of such a framework, pointing out the different difficulties at the theoretical and practical levels. The results so far obtained by combining modelling and data are very promising.

The particularity of our modelling approach is to choose models where the number of parameters and state variables is reduced to the minimum, in order to be compatible with clinical observations, and where we can interpret these parameters in a physiological manner. For instance, the calcium handling would be of great importance if we were using the model to simulate series of contractions (mostly above 10 contractions), where the dynamics of the calcium impacts the contraction. As the medical images we are using are a reconstruction on one heart beat (even if acquisitions are from several cycles), we believe that using a mean behaviour of calcium is reasonable.

Precise calibration of the model before data assimilation is difficult and additional measurements can help us with this task. Progress in MRI, especially in flow measurements, makes it conceivable to obtain patient-specific boundary conditions. Indeed, it seems important to have first an adjustment of the pre-load and after-load before looking further into local estimation. Simplified fluid-structure models coupled with velocity and distension measurements can give insights on how to adjust these global parameters. Defining the right mechanical interaction between atria, arteries, ventricles and the fibrous structure is complex. To solve this difficulty, we also plan to introduce some displacement boundary conditions on the base, extracted from the observations, to avoid having to simulate all the listed structures.

For data assimilation, the current work is on observation operators, for instance with tagged MR that can be written in a Lagrangian framework. Lagrangian approach is more easily dealt with, but it is not suitable for all types of measurements, such as cine MRI and ultrasound which are directly related to the deformed geometry. Many clinical observations are indeed more Eulerian in essence, and new methodology would need to be designed to deal with them.

Future developments are planned to integrate different modalities. For instance, with patients undergoing electrophysiology studies, electrophysiology clinical data can be acquired, using XMR interventional imaging for instance (Rhode et al., 2005). Such datasets make it possible to also initialise electrophysiology models of the myocardium (Sermesant et al., 2005). Having a patient-specific command of the contraction through a measure of the patient activation pattern would definitely help the data assimilation.

Finally, we point out that an interesting open problem concerns whether or not the electrical activity may also be estimated from displacements measurements of the myocardium. This proposed framework could give insights on this problem. Finally, coupling models and parameter estimation is valuable for interventional planning and therapy testing, owing to the predictive modelling capability. However, before achieving a clinical use of this framework, each step of this proof-of-concept will have to be thoroughfully validated and probably extended to cope with the quality and variability of clinical routine data.

Acknowledgements

The authors thank for their collaboration with the Cardiac MR Research Group in Guy's Hospital, London and the co-workers of the ICEMA collaborative research actions[4,5] funded by INRIA. Part of this work was done during the Summer Mathematical Research Centre on Scientific Computing and its Applications (CEMRACS).[6] The authors acknowledge grant support from EPSRC (M.S., O.C. and R.A.), from the Ministry of Education of the Czech Republic, Research Project MSM 4977751303 (R.C.), and the use of software developed by the Epidaure/Asclepios project,[7] INRIA.

This work is part of the INRIA Large Initiative Action CardioSense3D[8] launched in 2005.

References

Aletras, A., Ingkanisorn, W., Mancini, C., Arai, A., 2005. DENSE with SENSE. Journal of Magnetic Resonance 176 (1), 99–106.

Aliev, R., Panfilov, A., 1996. A simple two-variable model of cardiac excitation. Chaos, Solitons and Fractals 7 (3), 293–301.

Alpert, N., Bradshaw, J., Kennedy, D., Correia, J., 1990. The principal axis transformation – a method for image registration. Journal of Nuclear Medicine 31, 1717–1722.

Andriantsimiavona, R., Griffin, L., Hill, D., Razavi, R., 2003. Simple cardiac MRI segmentation. In: International Society for Magnetic Resonance in Medicine Scientific Meeting. vol. 6. p. 951.

Arts, T., Bovendeerd, P., van der Toorn, A., Geerts, L., Kerckhoffs, R., Prinzen, F., 2001. Modules in cardiac modeling: mechanics,

[4] http://www-rocq.inria.fr/who/Frederique.Clement/icema.html.

[6] http://smai.emath.fr/cemracs/cemracs04/index.php.

[7] http://www-sop.inria.fr/epidaure/index.php.

[8] http://www-sop.inria.fr/CardioSense3D/.

circulation, and depolarization wave. In: Functional Imaging and Modeling of the Heart (FIMH'01)No. 2230 in Lecture Notes in Computer Science (LNCS). Springer, pp. 83–90.

Axel, L., Montillo, A., Kim, D., 2005. Tagged magnetic resonance imaging of the heart: a survey. Medical Image Analysis 9 (4), 376–393.

Ayache, N. (Ed.), 2004. Computational Models for the Human Body. Ciarlet, P., (Series Ed.). Handbook of Numerical Analysis. Elsevier.

Bathe, K., 1996. Finite Element Procedures. Prentice-Hall.

Berr, S., Roy, R., French, B., Yang, Z., Gilson, W., Kramer, C., Epstein, F., 2005. Black blood gradient echo cine magnetic resonance imaging of the mouse heart. Magnetic Resonance in Medicine 53 (5), 1074–1079.

Bestel, J., Clément, F., Sorine, M., 2001. A biomechanical model of muscle contraction. In: Medical Image Computing and Computer-Assisted Intervention (MICCAI'01)Lecture Notes in Computer Science (LNCS), vol. 2208. Springer, pp. 1159–1161.

Blekas, K., Likas, A., Galatsanos, N., Lagaris, I., 2005. A spatially constrained mixture model for image segmentation. IEEE Transactions on Neural Networks 16 (2), 494–498.

Cerqueira, M., Weissman, N., Dilsizian, V., Jacobs, A., Kaul, S., Laskey, W., Pennell, D., Rumberger, J., Ryan, T., Verani, M., 2002. Standardized myocardial segmentation and nomenclature for tomographic imaging of the heart. Circulation 105, 539–542.

Chandrashekara, R., Mohiaddin, R., Rueckert, D., 2004. Analysis of 3-D myocardial motion in tagged MR images using nonrigid image registration. IEEE Transactions on Medical Imaging 23 (10), 1245–1250.

Chapelle, D., Clément, F., Génot, F., Tallec, P.L., Sorine, M., Urquiza, J., 2001. A physiologically-based model for the active cardiac muscle contraction. In: Functional Imaging and Modeling of the Heart (FIMH'01)No. 2230 in Lecture Notes in Computer Science (LNCS). Springer, pp. 128–133.

Chapelle, D., Sainte-Marie, J., Cimrman, R., 2004. Modeling and estimation of the cardiac electromechanical activity. In: Proceedings of the ECCOMAS 2004 Conference.

Chenoune, Y., Deléchelle, E., Petit, E., Goissen, T., Garot, J., Rahmouni, A., 2005. Segmentation of cardiac cine-mr images and myocardial deformation assessment using level set methods. Computerized Medical Imaging and Graphics 29 (8), 607–616.

Chui, C., Chen, G., 1999. Kalman Filtering With Real Time Applications. Springer-Verlag.

Costa, K., Holmes, J., McCulloch, A., 2001. Modelling cardiac mechanical properties in three dimensions. Philosophical Transactions of the Royal Society of London 359 (1783), 1233–1250.

Courtier, P., Talagrand, O., 1987. Variational assimilation of meteorological observations with the adjoint vorticity equation. Quarterly Journal of the Royal Meteorological Society 113, 1311–1347.

Eldar, M., Ohad, D., Goldberger, J., Rotstein, Z., Hsu, S., Swanson, D., Greenspon, A., 1997. Transcutaneous multielectrode basket catheter for endocardial mapping and ablation of ventricular tachycardia in the pig. Circulation 96 (7), 2430–2437.

Faris, O., Evans, F., Ennis, D., Helm, P., Taylor, J., Chesnick, A., Guttman, M., Ozturk, C., McVeigh, E., 2003. Novel technique for cardiac electromechanical mapping with magnetic resonance imaging tagging and an epicardial electrode sock. Annals of Biomedical Engineering 31 (4), 430–440.

FitzHugh, R., 1961. Impulses and physiological states in theoretical models of nerve membrane. Biophysical Journal 1, 445–466.

Frangi, A., Niessen, W., Viergever, M., 2001. Three-dimensional modeling for functional analysis of cardiac images: a review. IEEE Transactions on Medical Imaging 1 (20), 2–25.

Frangi, A., Radeva, P., Santos, A., Hernandez, M. (Eds.), 2005. Functional Imaging and Modeling of the Heart (FIMH'05). No. 3504 in Lecture Notes in Computer Science (LNCS). Springer.

Fung, Y., 1993. Biomechanics: Mechanical properties of Living Tissues, second ed. Springer-Verlag.

Geerts, L., Kerckhoffs, R., Bovendeerd, P., Arts, T., 2003. Towards patient specific models of cardiac mechanics: a sensitivity study. In: International Symposium on Surgery Simulation and Soft Tissue Modeling (IS4TM'03)No. 2230 in Lecture Notes in Computer Science (LNCS). Springer, pp. 00–11.

González Ballester, M., Zisserman, A., Brady, M., 2002. Estimation of the partial volume effect in MRI. Medical Image Analysis 6 (4), 389–405.

Grothues, F., Smith, G.C., Moon, J.C., Bellenger, N.G., Collins, P., Klein, H.U., Pennell, D.J., 2002. Comparison of interstudy reproducibility of cardiovascular magnetic resonance with two-dimensional echocardiography in normal subjects and in patients with heart failure or left ventricular hypertrophy. American Journal of Cardiology 90 (1), 29–34.

Guccione, J., McCulloch, A., 1991. Theory of Heart: Biomechanics, Biophysics, and Nonlinear Dynamics of Cardiac Function. Springer-Verlag, pp. 121–144 (Ch. Finite element modeling of ventricular mechanics).

Hill, A., 1938. The heat of shortening and the dynamic constants in muscle. Proceedings of the Royal Society of London (B) 126, 136–195.

Hsu, E., Henriquez, C., 2001. Myocardial fiber orientation mapping using reduced encoding diffusion tensor imaging. Journal of Cardiovascular Magnetic Resonance 3, 325–333.

Humphrey, J., 2002. Continuum biomechanics of soft tissues. Proceedings of the Royal Society of London A 459, 3–46.

Hunter, P., Pullan, A., Smaill, B., 2003. Modeling total heart function. Annual Review of Biomedical Engineering 5, 147–177.

Huxley, A., 1957. Muscle structure and theories of contraction. Progress in Biophysics and Biological Chemistry 7, 255–318.

Kacere, R., Pereyra, M., Nemeth, M., Muthupillai, R., Flamm, S., 2005. Quantitative assessment of left ventricular function: steady-state free precession MR imaging with or without sensitivity encoding. Radiology 235 (3), 1031–1035.

Kalman, R., 1960. A new approach to linear filtering and prediction problems. ASME Transactions – Journal of Basic Engineering 82 (Series D), 35–45.

Kalman, R., Bucy, R., 1961. New results in linear filtering and prediction theory. ASME Transactions – Journal of Basic Engineering 83 (Series D), 95–108.

Kano, H., Ghosh, B., Kanai, H., 2001. Single camera based motion and shape estimation using extended Kalman filtering. Mathematical and Computer Modelling 34 (5–6), 511–525.

Katila, T., Magnin, I., Clarysse, P., Montagnat, J., Nenonen, J. (Eds.), 2001. Functional Imaging and Modeling of the Heart (FIMH'01). No. 2230 in Lecture Notes in Computer Science (LNCS). Springer.

Kellerhals, B., 2001. Financial pricing models in continuous time and Kalman filtering. Lecture Notes in Economics and Mathematical Systems, 506.

Kilner, P., Yang, G., Wilkes, A., Mohiaddin, R., Firmin, D., Yacoub, M., 2000. Asymmetric redirection of flow through the heart. Nature 404, 759–761.

Knudsen, Z., Holden, A., Brindley, J., 1997. Qualitative modelling of mechano-electrical feedback in a ventricular cell. Bulletin of Mathematical Biology 6 (59), 115–181.

Kunz, R., Oellig, F., Krummenauer, F., Oberholzer, K., Romaneehsen, B., Vomweg, T., Horstick, G., Hayes, C., Thelen, M., Kreitner, K., 2005. Assessment of left ventricular function by breath-hold cine MR imaging: comparison of different steady-state free precession sequences. Journal of Magnetic Resonance Imaging 21 (2), 140–148.

Le Dimet, F., Talagrand, O., 1986. Variational algorithms for analysis and assimilation of meteorological observation: theoretical aspects. Tellus 38, 97–110.

Le Tallec, P., 1994. Handbook of Numerical Analysis. In: Ciarlet, P.G., Lions, J.L., (Eds.), vol. 3. North-Holland, pp. 465–622 (Ch. Numerical methods for nonlinear three-dimensional elasticity).

Liew, A., Yan, H., 2003. An adaptive spatial fuzzy clustering algorithm for 3-D MR image segmentation. IEEE Transactions on Medical Imaging 22 (9), 1063–1075.

Lin, D., Yin, F., 1998. A multiaxial constitutive law for mammalian left ventricular myocardium in steady-state barium contracture or tetanus. Journal of Biomechanical Engineering 120 (4), 504–517.

Lions, J., 1968. Contrôle optimal des systèmes gouvernés par des équations aux dérivées partielles. Dunod.

Lorensen, W., Cline, H., 1987. Marching cubes: a high resolution 3D surface reconstruction algorithm. Computer Graphics (Proc. of SIGGRAPH) 21 (4), 163–169.

Lorenzo-Valdés, M., Sanchez-Ortiz, G.I., Elkington, A.G., Mohiaddin, R.H., Rueckert, D., 2004. Segmentation of 4d cardiac mr images using a probabilistic atlas and the em algorithm. Medical Image Analysis 8 (3), 255–265.

MacDonald, D., 1974. Blood Flow in Arteries. Edward Harold Press.

MacLeod, R., Yilmaz, B., Taccardi, B., Punske, B., Serinagaolu, Y., Brooks, D., 2001. Direct and inverse methods for cardiac mapping using multielectrode catheter measurements. Journal of Biomedizinische Technik 46, 207–209.

Magnin, I., Montagnat, J., Clarysse, P., Nenonen, J., Katila, T. (Eds.), 2003. Functional Imaging and Modeling of the Heart (FIMH'03). No. 2674 in Lecture Notes in Computer Science (LNCS). Springer.

Masood, S., Yang, G., Pennell, D., Firmin, D., 2000. Investigating intrinsic myocardial mechanics: the role of MR tagging, velocity phase mapping and diffusion imaging. Journal of Magnetic Resonance Imaging 12 (6), 873–883.

McCulloch, A., Bassingthwaighte, J., Hunter, P., Noble, D., Blundell, T., Pawson, T., 1998. Computational biology of the heart: from structure to function. Progress in Biophysics and Molecular Biology 69 (2/3), 151–559.

Mercier, J., DiSessa, T., Jarmakani, J., Nakanishi, T., Hiraishi, S., Isabel-Jones, J., Friedman, W., 1982. Two-dimensional echocardiographic assessment of left ventricular volumes and ejection fraction in children. Circulation 65, 962–969.

Mirsky, I., Parmley, W., 1973. Assessment of passive elastic stiffness for isolated heart muscle and the intact heart. Circulation Research 33, 233–243.

Mitchell, S.C., Bosch, J.G., Lelieveldt, B.P., van der Geest, R.J., Reiber, J.H., Sonka, M., 2002. 3-D active appearance models: segmentation of cardiac MR and ultrasound images. IEEE Transactions on Medical Imaging 21 (9), 1167–1178.

Montagnat, J., Delingette, H., 2005. 4D deformable models with temporal constraints : application to 4d cardiac image segmentation. Medical Image Analysis 9 (1), 87–100.

Mulquiney, P., Smith, N., Clark, K., Hunter, P., 2001. Mathematical modelling of the ischaemic heart. Nonlinear Analysis 47, 235–244.

Osman, N., Kerwin, W., McVeigh, E., Prince, J., 1999. Cardiac motion tracking using CINE harmonic phase (HARP) magnetic resonance imaging. Magnetic Resonance in Medicine 42 (6), 1048–1060.

Pan, L., Prince, J.L., Lima, J.A., Osman, N.F., 2005. Fast tracking of cardiac motion using 3d-harp. IEEE Transactions on Biomedical Engineering 52 (8), 1425–1435.

Panfilov, A., Holden, A. (Eds.), 1996. Computational Biology of the Heart. Wiley, pp. 295–343 (Ch. Forward and Inverse Problems in Electrocardiography).

Papademetris, X., Sinusas, A.J., Dione, D.P., Duncan, J.S., 2001. Estimation of 3D left ventricle deformation from echocardiography. Medical Image Analysis 5 (1), 17–28.

Paragios, N., 2003. A level set approach for shape-driven segmentation and tracking of the left ventricle. IEEE Transactions on Medical Imaging 22 (6), 773–776.

Peters, D., Ennis, D., Rohatgi, P., Syed, M., McVeigh, E., Arai, A., 2004. 3D breath-held cardiac function with projection reconstruction in steady state free precession validated using 2D cine MRI. Journal of Magnetic Resonance Imaging 20 (3), 411–416.

Rhode, K., Sermesant, M., Brogan, D., Hegde, S., Hipwell, J., Lambiase, P., Rosenthal, E., Bucknall, C., Qureshi, S., Gill, J., Razavi, R., Hill, D., 2005. A system for real-time XMR guided cardiovascular intervention. IEEE Transactions on Medical Imaging 24 (11), 1428–1440.

Rohan, E., Cimrman, R., 2002. Sensitivity analysis and material identification for activated smooth muscle. Computer Assisted Mechanics and Engineering Science 9, 519–541.

Rohan, E., Whiteman, J., 2000. Shape optimization of elasto-plastic structures and continua. Computer Methods in Applied Mechanics and Engineering 187, 261–288.

Ryf, S., Spiegel, M., Gerber, M., Boesiger, P., 2002. Myocardial tagging with 3D-CSPAMM. Journal of Magnetic Resonance Imaging 16 (3), 320–325.

Sachse, F., 2004. Computational Cardiology: Modeling of Anatomy, Electrophysiology, and MechanicsLecture Notes in Computer Science, vol. 2966. Springer.

Sainte-Marie, J., Chapelle, D., Cimrman, R., Sorine, M., in press. Modeling and estimation of the cardiac electromechanical activity, Computers and Structures.

Sainte-Marie, J., Chapelle, D., Sorine, M., 2003. Data assimilation for an electro-mechanical model of the myocardium. In: Bathe, K. (Ed.), Second M.I.T. Conference on Computational Fluid and Solid Mechanics. pp. 1801–1804.

Schmitt, C., Zrenner, B., Schneider, M., Karch, M., Ndrepepa, G., Deisenhofer, I., Weyerbrock, S., Schreieck, J., Schomig, A., 1999. Clinical experience with a novel multielectrode basket catheter in right atrial tachycardias. Circulation 99 (18), 2414–2422.

Sermesant, M., Forest, C., Pennec, X., Delingette, H., Ayache, N., 2003. Deformable biomechanical models: application to 4D cardiac image analysis. Medical Image Analysis 7 (4), 475–488.

Sermesant, M., Rhode, K., Sanchez-Ortiz, G., Camara, O., Andriantsimiavona, R., Hegde, S., Rueckert, D., Lambiase, P., Bucknall, C., Rosenthal, E., Delingette, H., Hill, D., Ayache, N., Razavi, R., 2005. Simulation of cardiac pathologies using an electromechanical biventricular model and XMR interventional imaging. Medical Image Analysis 9 (5), 467–480.

Simonetti, O., Finn, J., White, R., Laub, G., Henry, D., 1996. Black blood T2-weighted inversion-recovery MR imaging of the heart. Radiology 199 (1), 49–57.

Stergiopulos, N., Westerhof, B., Westerhof, N., 1999. Total arterial inertance as the fourth element of the Windkessel model. American Journal of Physiology 276, H81–H88.

Tsao, J., Boesiger, P., Pruessmann, K., 2003. k-t BLAST and k-t SENSE: dynamic MRI with high frame rate exploiting spatio-temporal correlations. Magnetic Resonance in Medicine 50 (5), 1031–1042.

Ubbink, S., Bovendeerd, P., Delhaas, T., Arts, T., van de Vosse, F., 2006. Towards model-based analysis of cardiac MR tagging data: relation between left ventricular shear strain and myofiber orientation. Medical Image Analysis. Special Issue on FIMH.

Veronda, D., Westmann, R., 1970. Mechanical characterization of skin – finite deformation. Journal of Biomechanics 3, 114–124.